Electronic Supplementary Material (ESI) for Chemical Communications

Supporting information

Self-assembly of an asymmetrically functionalized [6]helicene at liquid/solid interfaces

Tatyana Balandina, Maarten van der Meijden, Oleksandr Ivasenko, David Cornil, Jérôme Cornil, Roberto Lazzaroni, Richard M. Kellogg, Steven De Feyter

1.STM experiments and chemicals

STM imaging was carried out at room temperature (20 - 24^{o} C) using a PicoSPM (Agilent) system operating in constant-current mode with the tip immersed in the supernatant liquid. STM tips were prepared by mechanical cutting of Pt/Ir wire (80%/20%, diameter 0.25 mm). As substrates, Au(111) films on mica (Georg Albert PVD Company) or highly oriented pyrolytic graphite (HOPG, grade ZYB, Advanced Ceramics Inc., Cleveland, USA) was used. Immediately prior their use Au(111) substrates were annealed in an oven. A fresh HOPG surface was prepared by removing the upper graphene layers with Scotch tape. Commercially available coronene (Aldrich Co.), 1-octanoic acid (Sigma Co., 99%), and 1,2,4-trichlorobenzene (Sigma-Aldrich Co., 99%) were used as solvents. In addition to well solubilize the helicenes, these solvents are appropriate liquids for STM imaging at the liquid-solid interface (non-conductive, low vapor pressure). For each measurement a 8 μL drop of the desired solution was applied directly to the freshly prepared substrate. STM imaging was carried out in the constant-current mode, and started immediately after drop casting.

5-Amino[6]helicene

1H NMR (DMSO-d6) δ8.12 (d, 1H), 7.93-8.05 (m, 3H), 7.89 (d, 1H), 7.82 (d, 1H), 7.49 (d, 1H), 7.46 (dd, 1H), 7.21 (t, 2H), 7.07 (s, 1H), 6.61-6.69 (dq, 2H), 6.13 (bs, 2H)

13C NMR (DMSO-d6) δ144.8, 136.7, 134.1, 131.9, 131.6, 131.2, 130.1, 128.3, 128.1, 127.7, 127.1, 126.8, 126.0, 125.7, 125.4, 125.1, 124.5, 124.3, 122.7, 120.6, 104.0, 98.1, 91.6

[M+1](API/ES) calculated: 344.14 found: 344.1 CD data for 5-Amino-hexahelicene with an e.e. of 99% and a chemical purity of 93%

$\Delta\varepsilon = \Theta / (32980 * c * l) = 55.1/(32980x0.000013x1) = 128.5$ mdeg/mol/l/cm at 248 nm and -35.0/(32980x0.000013x1) = -81.6 mdeg/mol/l/cm at 334 nm with a concentration of 0.013 mmol/L in MeOH

The compound oxidizes readily on exposure to air to give strongly colored material(s), likely due to oxidation of the amino group. This makes the purity determinations by HPLC difficult to interpret, since traces of strongly colored materials can give rise to large peaks in the HPLC using UV detection. This was tested by measuring one HPLC sample immediately after chromatography. HPLC analysis indicated a purity of 95%. When the sample was left overnight and measured again, the purity of the same sample as determined by HPLC had deteriorated to 90%, although no impurities could be seen in the 1H NMR spectra.

The material used had a purity >95% for the (-)-enantiomer and >90% for the (+)-enantiomer according to NMR analysis, and an e.e. >99% for the (-)-enantiomer and >96% for the (+)-enantiomer

The details for two batches, based on HPLC data and NMR spectra, are given. Batch 1 was used chiefly for exploratory STM work whereas highly purified batch 2 was used for final work

The analytical data may be summarized as follows:

Batch 1

Peak 1 ((M)-(-)-enantiomer):
93-95% pure according to HPLC
>95% pure according to NMR
>99% e.e. according to chiral HPLC

Peak 2 ((P)-(+)-enantiomer):
84-90% pure according to HPLC
Ca 95% pure according to NMR
>96% e.e. according to chiral HPLC

Batch 2

Peak 1 ((M)-(-)-enantiomer):
>98% pure according to HPLC
>95% pure according to NMR
>99% e.e. according to chiral HPLC

Peak 2 ((P)-(+)-enantiomer):
>95% pure according to HPLC
>95% pure according to NMR
>96% e.e. according to chiral HPLC

2.Details of the DFT calculations and STM simulations

DFT calculations were performed at the Density Functional Theory (DFT) level using the SIESTA (Spanish Initiative for Electronic Simulation with Thousands of Atoms) code. The valence electrons are described using a numerical atomic orbital basis set (double zeta + polarization) and the valence-core interactions are described with the pseudopotential method following the Troullier-Martins scheme. The calculations have been carried out within the Generalized Gradient Approximation (GGA) using the PBE exchange-correlation functional to get optimized geometries and electronic densities, upon which the VDW-DFT functional was applied. The gold surface was modeled using a slab based on 5 layers on metal atoms whereas 2 layers of carbon atoms were used to represent the graphite surface. For calculations on a single helicene molecule on gold, we used a $(\sqrt{21} \times \sqrt{21})R10.9$ unit cell with lattice vectors a = b = 13.56 Å. The calculations on dimers were performed by doubling the unit cell along one direction. For the single helicene molecule on graphite, we considered a surface equivalent to 5 × 5 the fundamental unit cell of graphite with lattice vectors a = b = 12.30Å. Periodic

boundary conditions were applied along the three dimensions with a vacuum space of ca. 20 Å introduced along the z direction to minimize interactions between superimposed slabs. In addition, a dipole sheet was incorporated in the middle of the vacuum to cancel artifacts due to dipole-dipole interactions.

The adsorption energies were calculated on the optimized structure where helicene molecules and the top two layers of the gold surface were allowed to relax fully. For calculations on graphite, the helicene molecule in the appropriate orientation (N-up or N-down) was positioned co-facially to the underlying graphite lattice and was fully relaxed while the substrate atoms were fixed. The adsorption energies were BSSE-corrected. Unfortunately, it was not possible to take solvent molecules into account due to very high costs and complexity of such calculations.

The optimization of H-bonding complex between AH and acetic acid (mimicking corresponding interactions with octanoic acid) was performed using Gaussian G09 software[1] at the B97D/cc-pvtz//B97D/cc-pvdz level of theory.

The simulations of the STM images were computed using the LDOS obtained from the SIESTA calculations using the WSxM software developed by Nanotec.[2]

3.DFT modeling and adsorption energies of M-AH on Au(111).

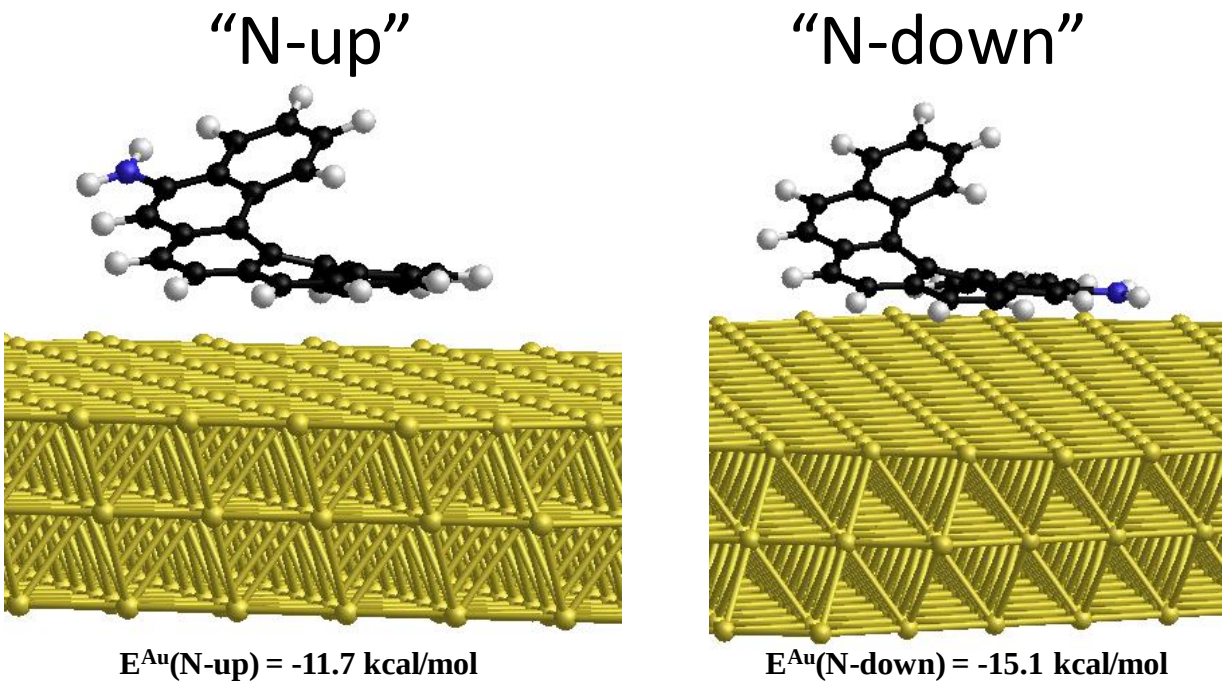

Fig. S1 DFT modeling and adsorption energies of M-**AH** on Au(111) in two different orientations: with $-NH_2$ group away from and close to the surface.

4.Representative STM images of assemblies of pure M-AH and P-AH.

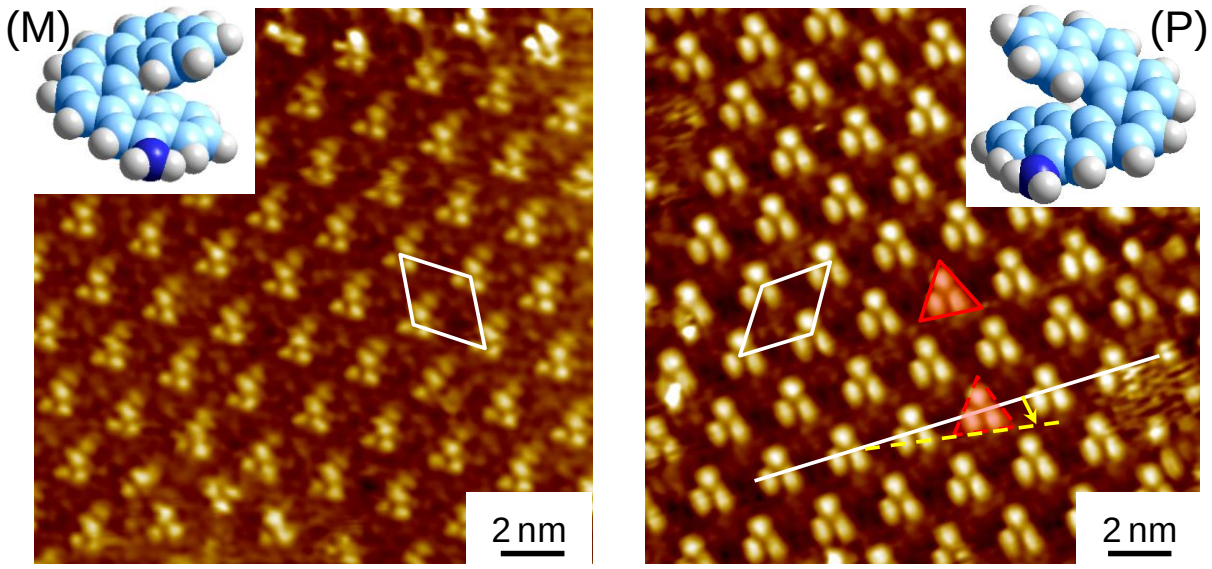

Fig. S2 Self-assembly of M-**AH** and P-**AH** at the interface between TCB and Au(111) surface. Left: STM image of *p3*-(M_3) network acquired at I_{set} = 300 pA, V_{set} = – 400 mV. Right: STM image of *p3*-(P_3) network acquired at I_{set} = 80 pA, V_{set} = – 350 mV.

5. Justification of the proposed structural model of *p6*-(**AH**$_{12}$) polymorph.

Several distinct structures of the unit cell are possible for *p6*-(**AH**$_{12}$) polymorph. Helicene hexamers in a half-cell are composed from 1) racemic dimers (discussed in details in the main text), 2) enantiomeric hexamers M_6 and P_6, 3) asymmetric hexamers (e.g. P_5M, M_4P_2 etc.) and 4) random composition. Observed C_3 symmetry of the helicene hexamers (half-cell) allows ruling out random composition as well as any asymmetry incompatible with C_3 rotation in the structure of the hexamers both in composition (P_5M, M_4P_2 etc.) as well as orientation of the helicenes (e.g. MMMPPP, MMPPMP etc.).

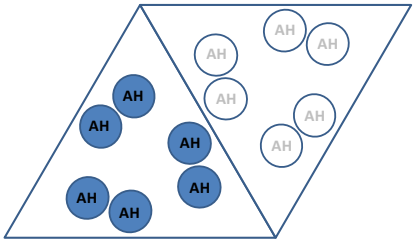

Possible structures of the half-cell:
1)MP-MP-MP
2)MM-MM-MM (and PP-PP-PP in the other half-cell)
3)Specific asymmetric arrangement: MM-MM-MP, MM-MP-PM, etc.
4)Completely random

In the self-assembly of racemic samples we have often observed very small patches of *p6*-(**AH**$_{12}$): down to single hexamer (Fig. S3). If *p6*-(**AH**$_{12}$) polymorph was build from M6 and P6 hexamers then such isolated hexamers should have been also observed in the self-assembly of pure enantiomers. This is not the case, thus leaving the only possibility that *p6*-(**AH**$_{12}$) is a racemic polymorph build from MPMPMP helicene hexamers.

Interestingly, the guests have well-defined localization within the chiral environment of the pores, suggesting possible enantioselective adsorption (e.g. P_3@*p6*-(M_6P_6) as opposed to random mixture P_nM_{3-n}@*p6*-(M_6P_6)).

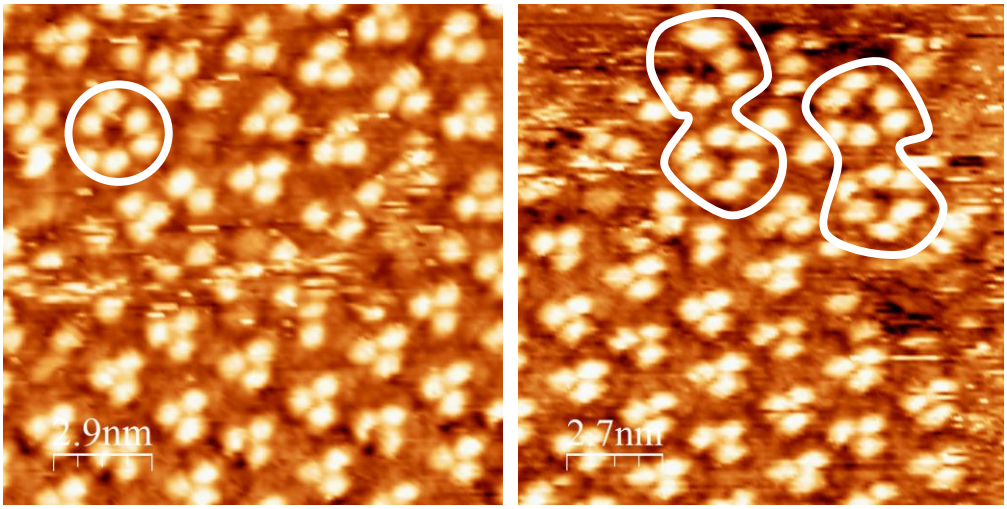

Fig. S3 STM images showing very small fragments of *p6*-(**AH**$_{12}$) polymorph observed only in the self-assembly of racemic MP-**AH** on Au(111) surface. Tunneling conditions: I_{set} = 95 pA, V_{set} = – 400 mV.

6. Structural defects due to kinetic trapping in MP-AH assemblies on Au(111) surface found even at sub-monolayer coverage.

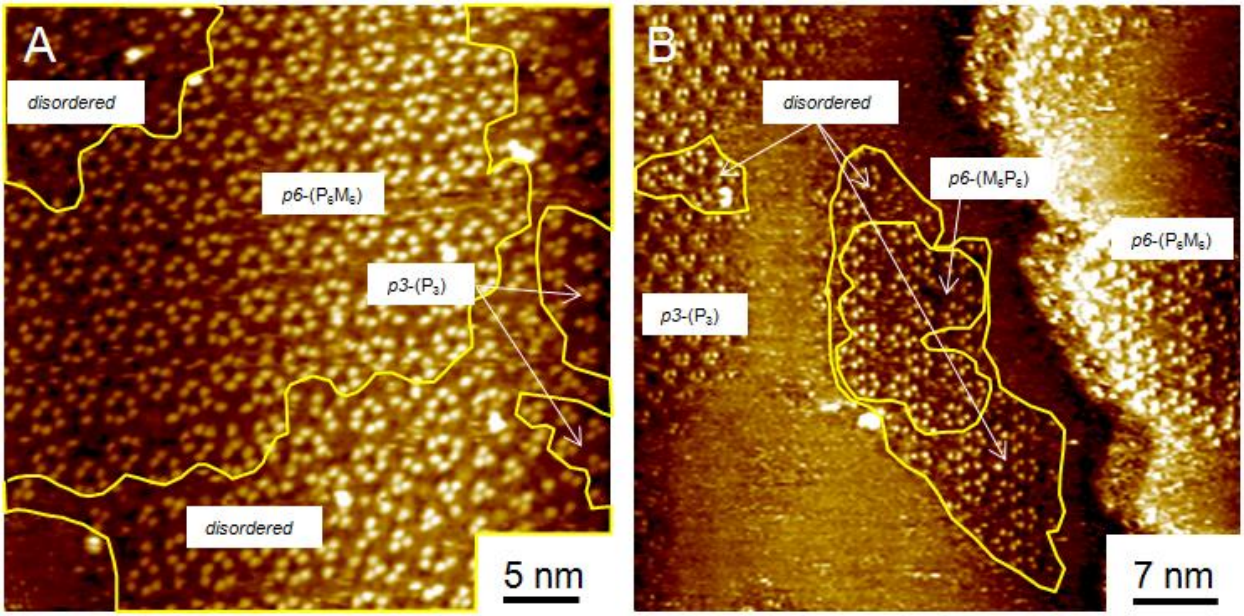

Fig. S4 STM images showing structural defects in self-assembly of MP-**AH** at the interface between TCB and Au(111) surface. Tunneling conditions: **A)** I_{set} = 95 pA, V_{set} = – 400 mV. **B)** I_{set} = 116 pA, V_{set} = – 400 mV.

7.DFT optimized structures and energies of homo- and heterochiral AH dimers on Au(111).

Table 1. DFT optimized energies of homo-(MM and PP) and heterochiral (MP) **AH** dimers.

	Energy per dimer			Energy per molecule	
	PBE [eV]	**VDW [eV]**	**PBE+VDW**	**[eV]**	**[kcal/mol]**
MM or PP	-0.73	-1.55	-2.28	-1.14	-26.29
MP	-0.69	-1.48	-2.16	-1.07	-24.67

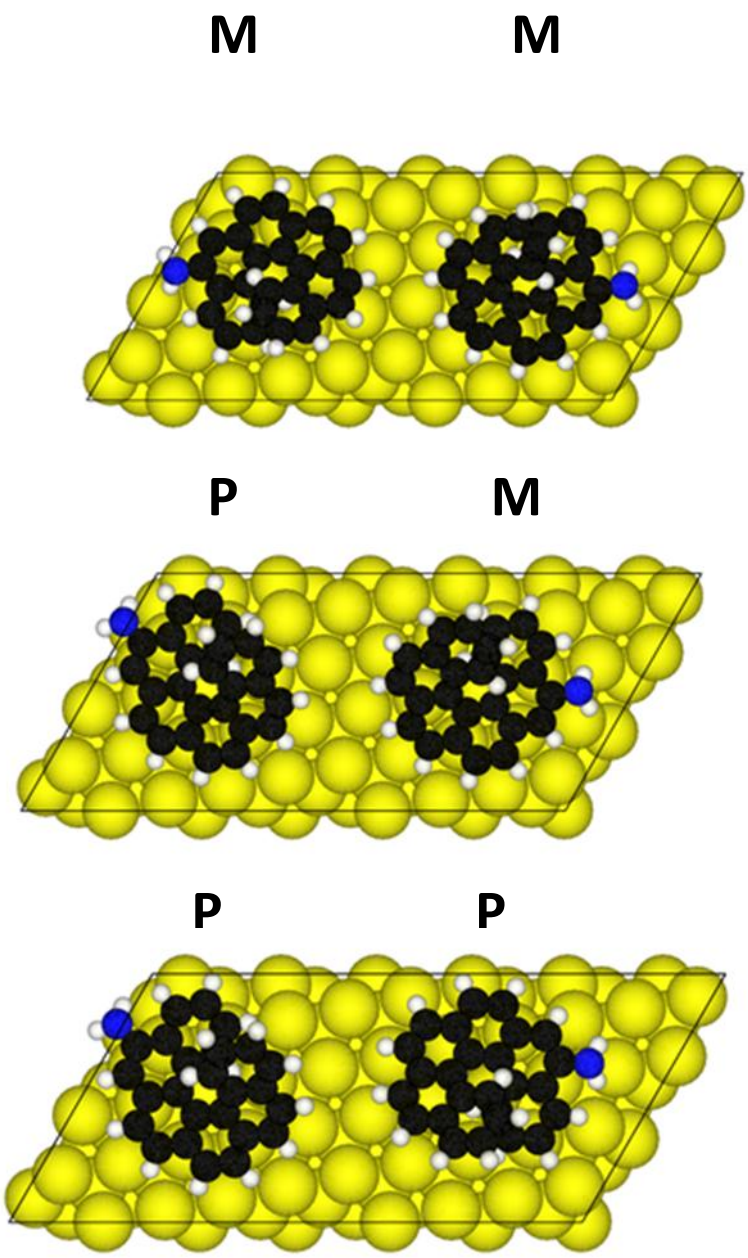

Fig. S5 DFT optimized structures of homo-(MM, PP) and heterochiral (MP) **AH** dimers on Au(111).

8.Projected densities of states (PDOS) of Au(111) surface decorated with N-up or N-down AH.

Adsorbed molecules are known to modify surface properties.[3] The calculations predict differences in dipole moments as well as densities of states of the Au(111) surface decorated with helicenes in N-up or N-down orientations. Currently, we are examining factors governing molecular orientation of the helicenes as well as complementary characterization of the helicene assemblies with different adsorption geometries and their properties.

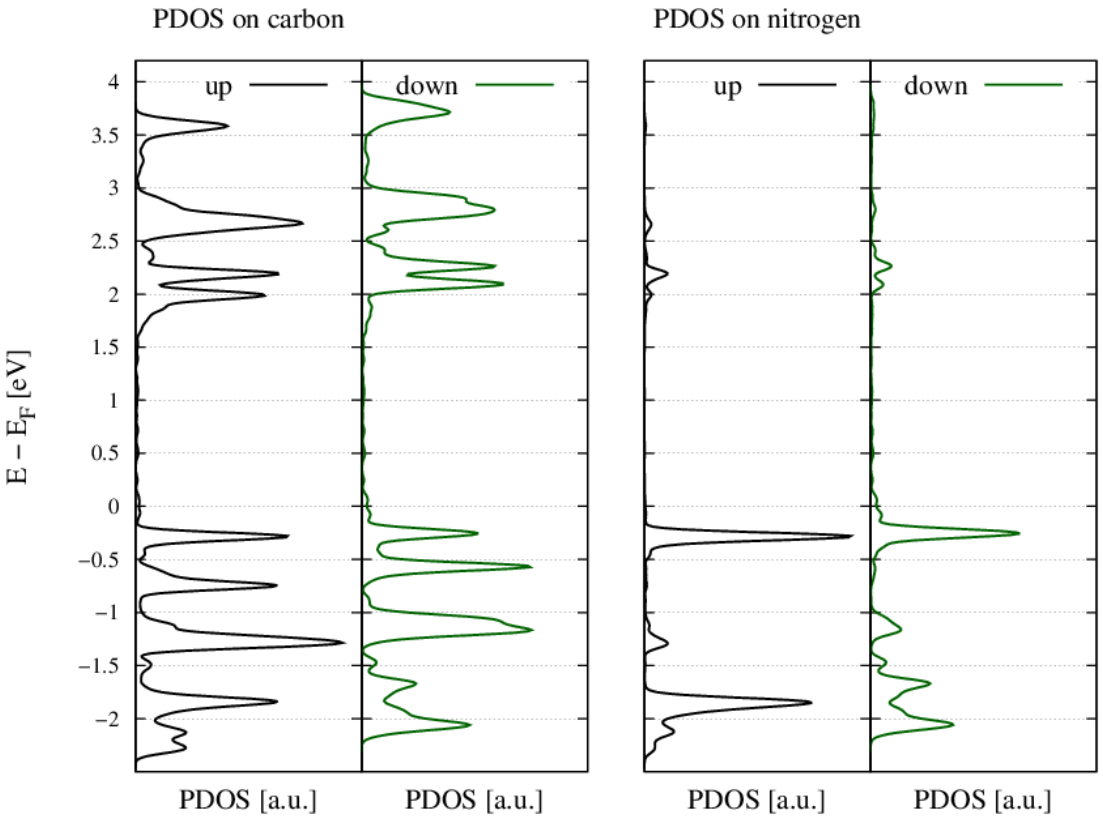

Fig. S6 PDOS of Au(111) surface decorated with N-up or N-down helicene.

9. Changes in gold work function associated with different adsorption geometries of AH.

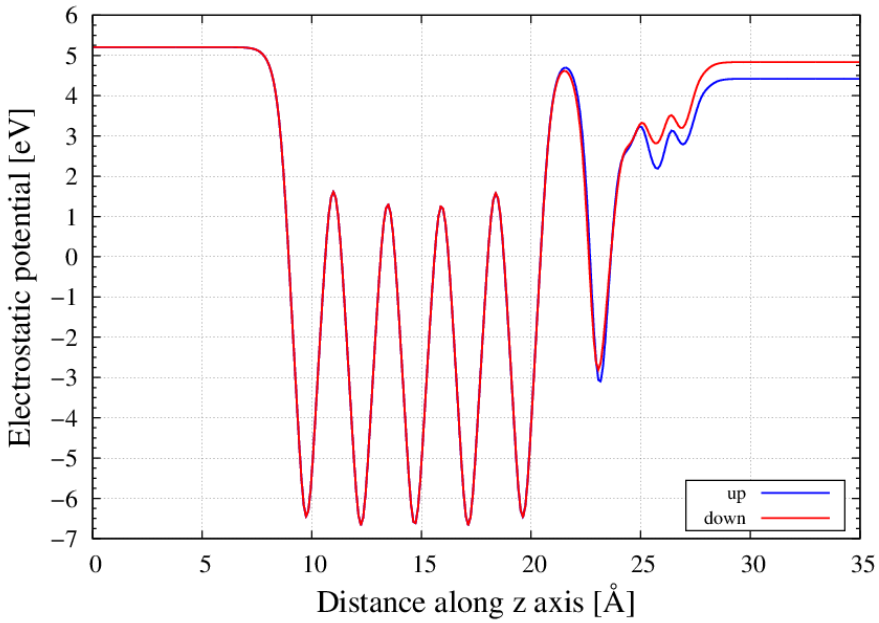

Fig. S7 Changes in gold work function associated with different adsorption geometries of AH.

Table 2. Changes in gold work function associated with different adsorption geometries: up-AH and down-AH.

	Φ_{Au}	Φ_{Sys}	$\Delta\Phi$	$\Phi_{Hél}$	BD
Up N-helicene	5.20	4.42	-0.78	-0.30	-0.48
Down N-helicene	5.20	4.83	-0.37	+0.22	-0.59

Φ_{Au} is calculated work function of gold, Φ_{Sys} the work function of the full system, and $\Delta\Phi$ the change in the work function upon helicene deposition. Φ_{hel} is the contribution to this shift arising from the dipole supported by the molecular backbone and **BD** from the bond dipole induced by interfacial electronic reorganization processes.[4] All values in eV.

10. Distribution of surface dipole moments in self-assembly of AH on Au(111) surface.

Table 3. Dipole moments along the z-axis, calculated on the optimized helicene/gold structures.

	μ_{tot}	μ_{hel}	μ_{int}
N-up helicene	3.31	1.27	2.04
N-down helicene	1.57	-0.95	2.52

μ_{tot} : dipole moment of the helicene/gold system ; **μ_{hel}** : dipole moment of the free helicene when removing the surface : **μ_{int}** : **$\mu_{tot} - \mu_{hel}$**. All values in Debye.

11. Co-assembly of P-AH and TMA on HOPG when deposited from octanoic acid solutions.

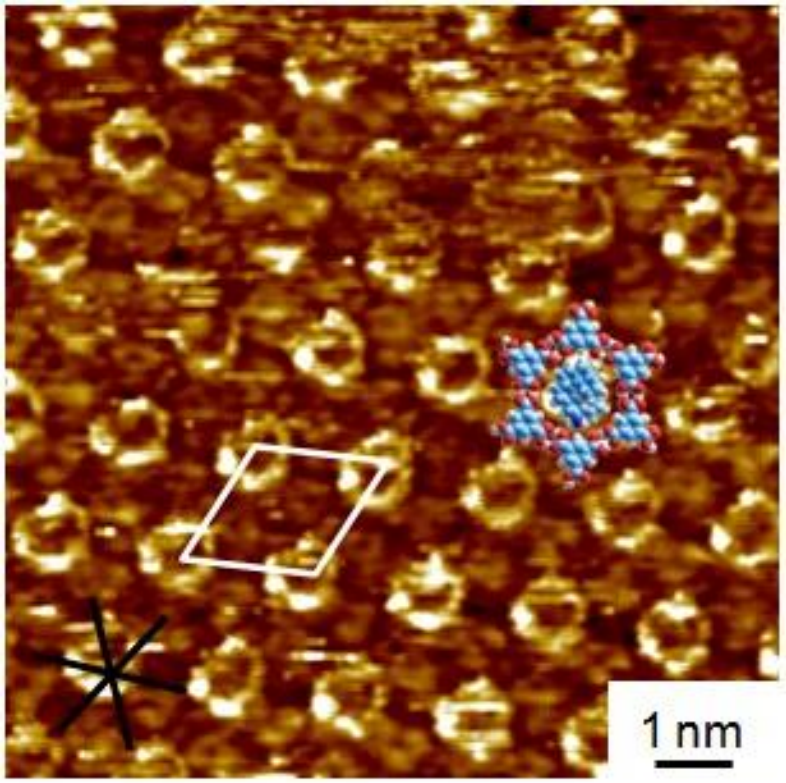

Fig. S8 STM image of **AH***@p6mm*-(**TMA_2**) host-guest network at the octanoic acid/HOPG. C_{AH} = 2,6 × 10^{-4} M and saturated solution of TMA. Tunneling parameters: I_{set} = 150 pA, V_{set} = – 1000 mV. In the model: carbon-blue, hydrogen-white, nitrogen- dark blue and oxygen-red.

12. DFT optimized structures and energies of different adsorption geometries of AH on HOPG.

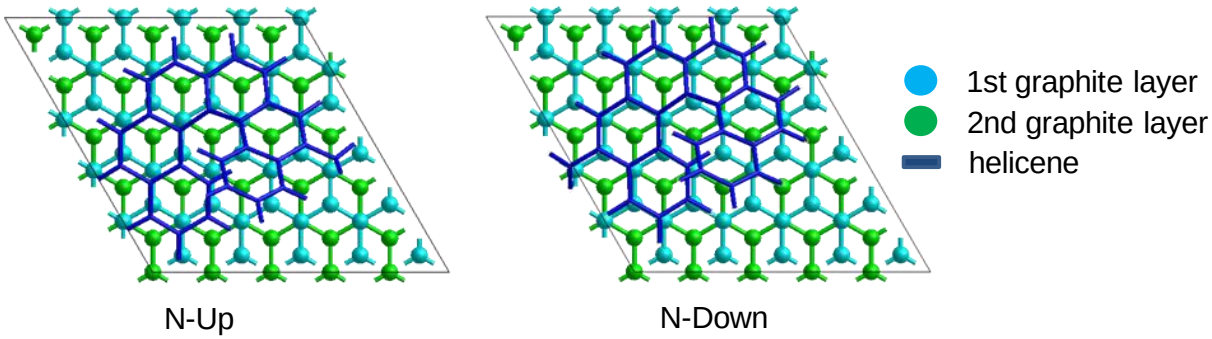

Fig.S9 DFT optimized structures of N-up and N-down orientations of **AH** on HOPG.

Table 4. DFT optimized energies of N-up and N-down orientations of **AH** on HOPG.

	Eads / eV (kcal/mol)		
	PBE	**VDW**	**PBE+VDW**
Up N-helicene	-0.07	-1.62	-1.69 (39.0)
Down N-helicene	-0.04	-1.67	-1.71 (39.4)

13. DFT optimized geometry and energy of H-bonding between AH and acetic acid (as a model system to describe H-bonding of AH with octanoic acid).

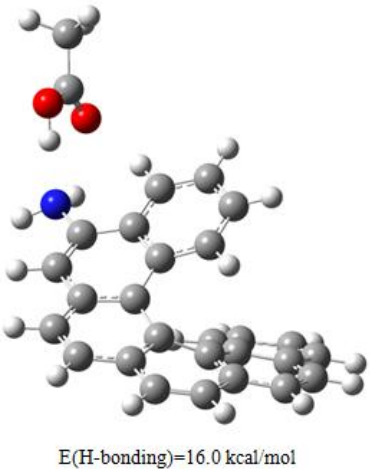

Fig.S10 DFT optimized geometry of hydrogen−bonding between AH and acetic acid.

14. An STM image of atypical defects in TMA network and corresponding molecular model of H-bonding between TMA and AH.

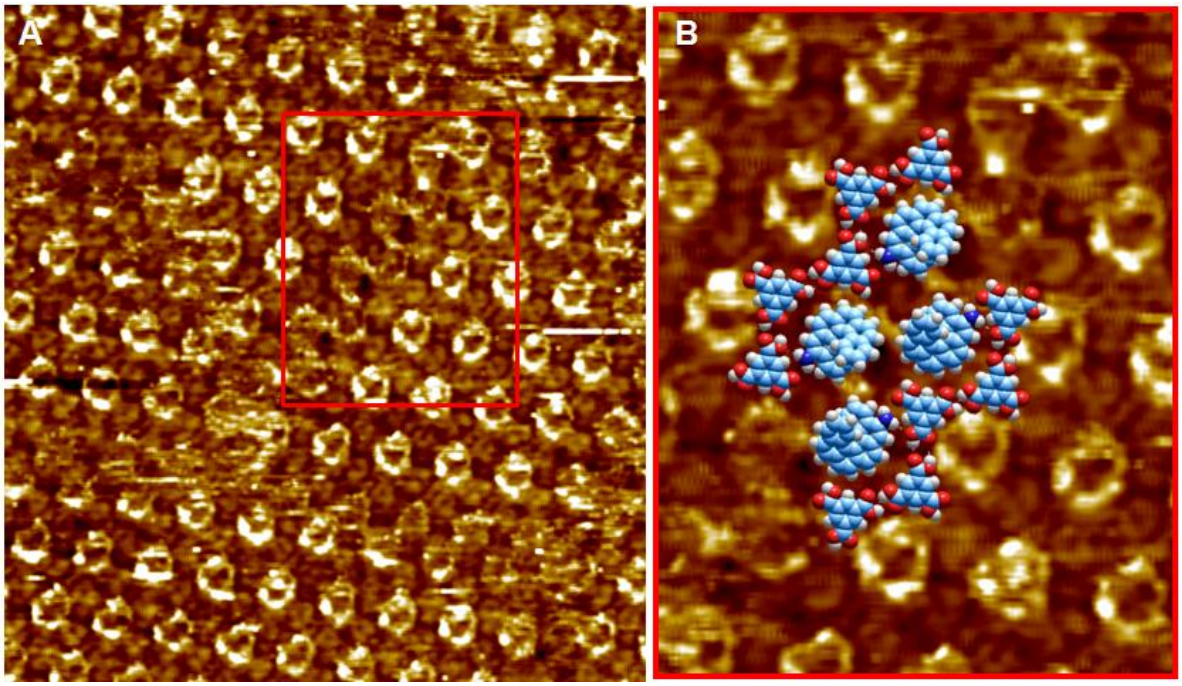

Fig. S11 Atypical defects in **AH***@p6mm*-(**TMA_2**) host-guest network at the octanoic acid/HOPG. C_{AH} = 2.6 × 10^{-4} M, saturated solution of TMA. Tunneling parameters: I_{set} = 150 pA, V_{set} = – 1000 mV. In the model: carbon-blue, hydrogen-white, nitrogen- dark blue and oxygen-red.

15. Design of co-assembly of aminohelicene with coronene on Au(111)

Weak intermolecular interactions and the strong substrate-directed nature of self-assembly of **AH** can be used to form more complex multi-component architectures. As an example we have investigated the co-assembly of M-**AH** and coronene (**COR**). The latter was chosen since it has a footprint and an adsorption energy similar to **AH**.[5]

Application of a TCB solution of both components (M-AH/COR ratio in solution was 5.8) to a clean Au(111) surface results in the formation of large domains of a uniform **COR***@p6*-(M_6) co-assembly (Fig. S12A). Here, M-**AH** trimers self-organize into a homochiral honeycomb structure with a single coronene molecule at the centre of each comb (Fig. S12B). In the STM images the coronenes are localized and well-resolved even though their diameter (~1.1 nm) is much smaller than that of the honeycomb pores (~1.9 nm). This highlights the strong site-selective binding of coronene molecules to the gold surface and absence of any significant helicene-coronene interactions. Interestingly, co-adsorption of coronene stabilizes the host network: only small patches of empty helicene honeycombs were observed on self-assembly from diluted TCB solutions of pure M-**AH** (Fig. S13).

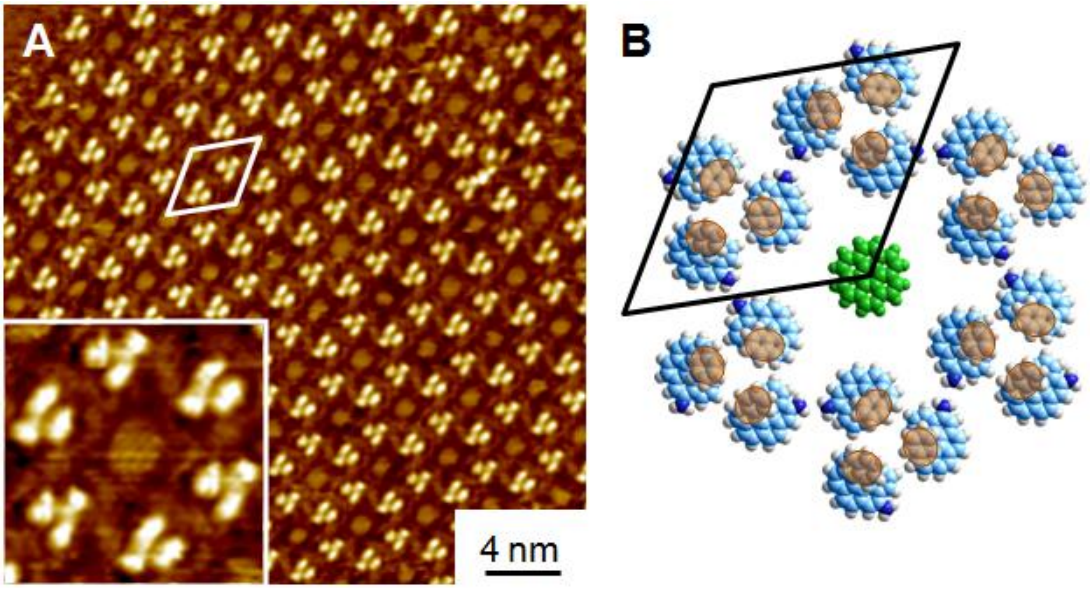

Fig. S12 **A)** an STM image and **B)** corresponding molecular sketch of bi-component co-assembly of M-**AH** ($C_{M\text{-}\mathbf{AH}}$ = 4,2 × 10^{-4} M) and **COR** ($C_{\mathbf{COR}}$ = 7.2 × 10^{-5} M) on the Au(111) surface. Tunneling parameters: I_{set} = 350 pA, V_{set} = – 352 mV. In the sketch: the coronene molecule is highlighted in green. Carbons, hydrogens and nitrogens of helicenes are light blue, white and dark blue, respectively.

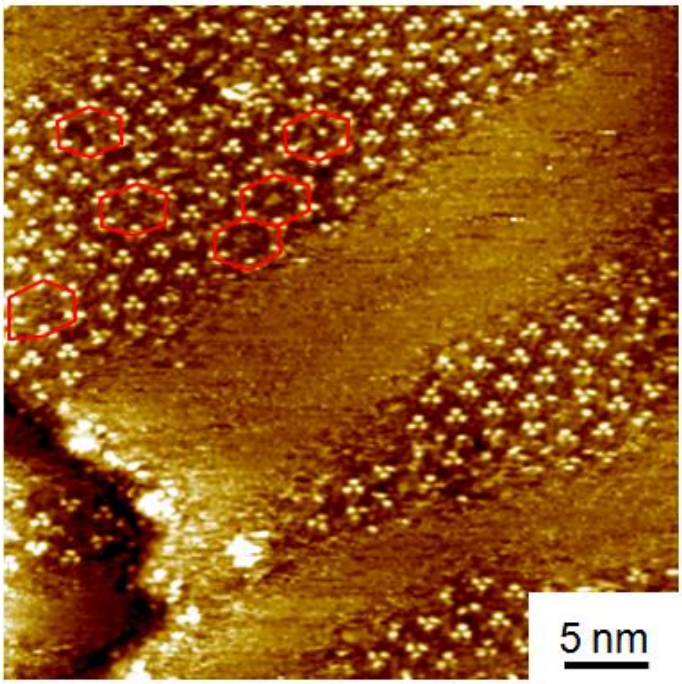

Fig. S13 STM image showing inclusion of honeycomb structural defects within *p3*-(M_3) domains upon self-assembly of M-**AH** at the TCB/Au(111) interface. Tunneling conditions: I_{set} = 267 pA, V_{set} = –400 mV.

[1] Gaussian 09, Revision **A.02**, M. J. Frisch, G. W. Trucks, H. B. Schlegel, G. E. Scuseria, M. A. Robb, J. R. Cheeseman, G. Scalmani, V. Barone, B. Mennucci, G. A. Petersson, H. Nakatsuji, M. Caricato, X. Li, H. P. Hratchian, A. F. Izmaylov, J. Bloino, G. Zheng, J. L. Sonnenberg, M. Hada, M. Ehara, K. Toyota, R. Fukuda, J. Hasegawa, M. Ishida, T. Nakajima, Y. Honda, O. Kitao, H. Nakai, T. Vreven, J. A. Montgomery, Jr., J. E. Peralta, F. Ogliaro, M. Bearpark, J. J. Heyd, E. Brothers, K. N. Kudin, V. N. Staroverov, R. Kobayashi, J. Normand, K. Raghavachari, A. Rendell, J. C. Burant, S. S. Iyengar, J. Tomasi, M. Cossi, N. Rega, J. M. Millam, M. Klene, J. E. Knox, J. B. Cross, V. Bakken, C. Adamo, J. Jaramillo, R. Gomperts, R. E. Stratmann, O. Yazyev, A. J. Austin, R. Cammi, C. Pomelli, J. W. Ochterski, R. L. Martin, K. Morokuma, V. G. Zakrzewski, G. A. Voth, P. Salvador, J. J. Dannenberg, S. Dapprich, A. D. Daniels, Ö. Farkas, J. B. Foresman, J. V. Ortiz, J. Cioslowski, and D. J. Fox, Gaussian, Inc., Wallingford CT, 2009.

[2] I. Horcas, R. Fernandez, J.M. Gomez-Rodriguez, J. Colchero, and J. Gomez-Herrero, *Rev. Sci. Instrum.*, 2007, **78**, 013705

[3] P. M. Holmblad, J. H. Larsen, I. Chorkendorff, *J. Chem. Phys.*,1996, **104**, 7289; F. P Zamborini, R. M. Crooks, *Langmuir*, 1998, **14**, 3279; A. Bansal, X. L. Li, S. I. Yi, W. H. Weinberg, N. S. Lewis, *J. Phys. Chem. B*, 2001, **105**, 10266.

[4] G. Heimel, L. Romaner, E. Zojer, and J-L Brédas, *Acc. Chem. Res.*, 2008, **41**, 721

[5] P. V. C. Medeiros, G. K. Gueorguiev and S. Stafström, *Phys. Rev. B*, 2012, **85**, 205423.